EUROPEAN ORGANIZATION FOR NUCLEAR RESEARCH

SPSC/P 73-1/Add.
8 January 1974

STATUS REPORT

PROPOSAL SPSC/P 73-1 TO STUDY HIGH-ENERGY NEUTRINO INTERACTIONS AT THE SPS

CERN, Dortmund, Heidelberg and Saclay Collaboration

I. INTRODUCTION

Since our proposal was submitted in July 1973 and while waiting for approval of the SPS Committee, we have continued to work on the design and preparation of the experiment, since we are of the opinion that such a large experiment is difficult to mount in the available time. This report gives some of the results of this work, as regards the design of the apparatus, the understanding of the properties of the apparatus and the physics that can be done with it. In the last part of the report we attempt to make some comparisons of the capabilities of this proposal and proposal SPSC/P 73-3.

The apparatus consists of two parts: a hadron shower detector and a combined heavy target muon spectrometer. For the latter we make no changes in the original design, but report the progress in the design of magnet units and drift chambers.

For the hadron shower detector we have also largely stuck to the proposal, but have changed the width of the scintillator slabs and the way in which the scintillators are combined on the same phototube. At the expense of electronic complication and added cost, this makes two important improvements possible: (a) the measurement of the spatial distribution of the shower, especially the angle of the shower and therefore its transverse momentum; (b) the differential measurement of the initial π^0 contribution to the shower, permitting an improvement in the hadron energy resolution.

II. HADRON SHOWER DETECTOR

A) Mechanical design of module

The mechanical design has been completed and is shown in Fig. 1. Each module consists of eighteen 3 cm steel plates with 1 cm gaps for the scintillator. Eight such modules are required for the total thickness given in the proposal.

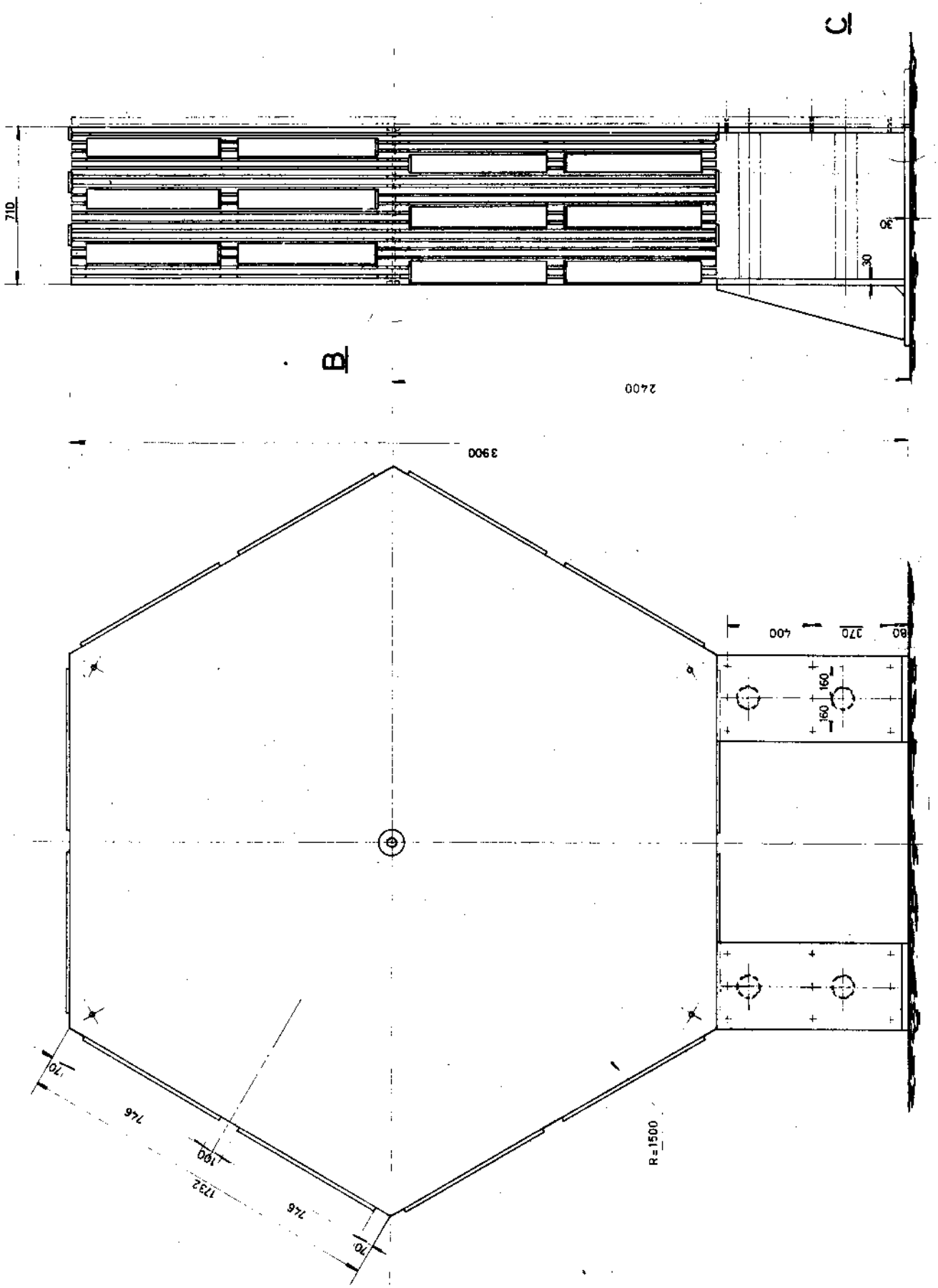

Fig. 1 A module of the hadron shower detector

B) Geometry of scintillators

The disposition of the scintillator has been improved with respect to the original design. The material and the thickness (0.6 cm) remain unchanged, but the strip width is reduced to 7.5 cm and the sequence of orientation is as follows: two layers horizontal followed by two layers rotated in one sense by 60°, followed by two layers rotated 60° in the other sense.

The strips are cut in the middle of the shower detector, and the end is covered with aluminium to reflect the light. The whole hadron detector is enclosed in a light-tight box; no provision for light tightness (wrapping, etc.) is provided for individual strips, except an aluminium foil covering for mechanical protection. Two adjacent strips are viewed by one photomultiplier through moulded light guides (Fig. 2). The output of this phototube is mixed with that of the opposite tube into a single channel, so that there are altogether $40 \times 2 \times 18 \times 8 = 11{,}520$ scintillator strips, seen by 5,760 phototubes, feeding 2,880 pulse height channels. Although the total scintillator area is the same, the number of pulse-height channels has increased by a factor eight. The increased resolution along the beam axis will make it possible to separate the π^0 contribution from the rest of the original hadron shower and thus provide the possibility of improved energy resolution. The increased resolution in the transverse dimension will make it possible to study the spatial structure of the shower, such as the average angle, and possibly to distinguish showers moving in different directions (e.g. from hadronic W decay), to the extent that the statistical nature of the shower development permits this.

C) Circuits

Pulse-height recording is fairly standard. An economic solution has been found giving special attention to the following essential requirements:

- high sensitivity to allow the use of cheap phototubes;
- dynamic range at least 1:500 to cover pulse heights from minimum ionizing particles and electromagnetic showers with high track density;

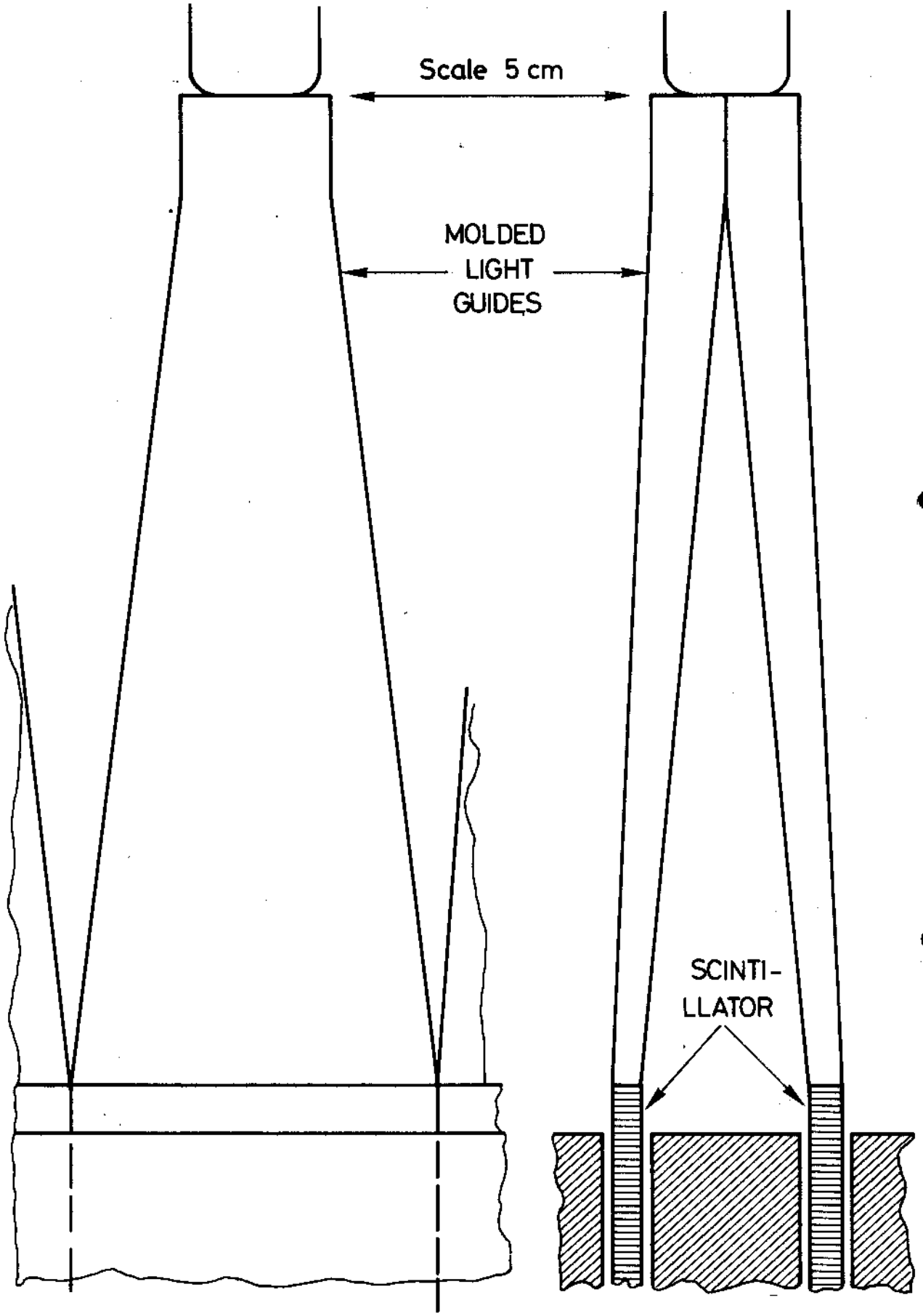

Fig. 2 Light guide construction for the scintillators in the hadron shower detector

- dead-time of 2-3 μs and sufficient buffer space to record several events in a short burst at full beam intensity.

A design based on a commercial hybrid charge-to-time converter has been tested successfully. The high dynamic range at short dead-time is obtained by employing a 100 MHz clock frequency and a non-linear discharge current. Apart from the charge-to-time converter which replaces the pre-amplifier, the circuit is logically equivalent to the drift-chamber time-digitizer (see § 6 of the proposal). A fraction of the specified dead-time is required to store all data (8 bits per channel) in cheap MOS memories. Redundant information (empty pulse-height channels) can be easily suppressed by software in between machine bursts before writing on magnetic tape.

The design of the electronic circuits is clearly not final. Based on the current ideas, the cost should be about 250 SF per channel. A second solution, using analog storage devices and possibly cheaper, is studied in parallel.

D) Layout of STAC as a whole

The arrangement of the modules in the complete detector is shown in Fig. 3. Two drift chambers are inserted, to permit an earlier measurement of the muon angle for those events originating in the upstream module.

The total weight of the STAC is 275 tons. The effective, fiducial weight for neutrino reactions will be less. It is necessary to reserve a downstream portion of $\sim$ 6 mean-free path (100 cm Fe) for shower development, and a margin on the side for the lateral spread of the shower, as well as the shower production angle, typically $\sim$ 100 mrad. Taking away therefore, 140 g/cm^2 (23 cm) on the lateral borders we are left with a fiducial weight of $\sim$ 150 tons. The average density of the detector is 5.6. In Table I we compare these figures with those of the detectors presently used in NAL. The fiducial weight is substantially (factor 3) greater than that of the largest hadronic shower detector at NAL. The ratio fiducial/total weight is also better because of the high density which is achieved.

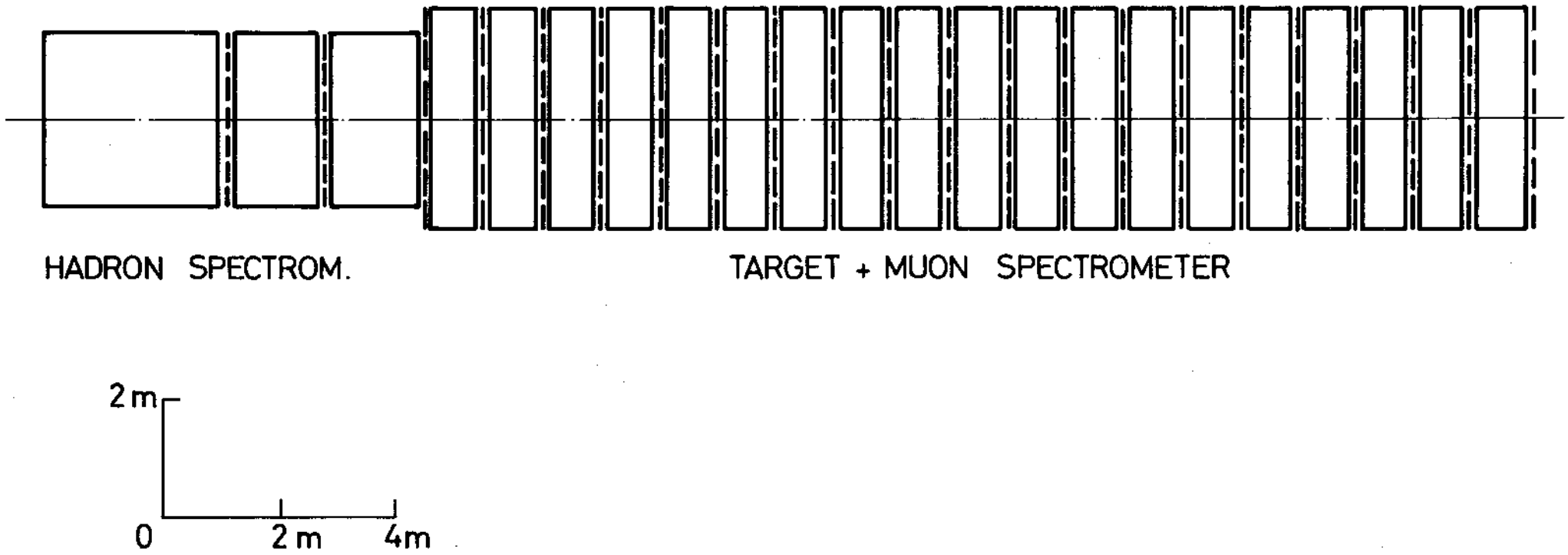

Fig. 3 Layout of the detector

TABLE I

Comparison of hadron shower detectors in present use at NAL with the one proposed here. For comparison, the calculation of fiducial volume is made on the basis of having six nuclear mean free paths downstream for shower development, and one nuclear mean-free path on the edge for lateral shower development. We wish to emphasize that this definition is of course quite arbitrary and is used for comparison only. Each experimental group will, in general, have its own, equally valid, definition of fiducial volume.

	Weight brutto (tons)	Length (metres)	Fiducial weight (tons)	Average density	Ratio fiducial / Brutto weight
15' H.L.B.C.	20	$\sim$ 5	$\sim$ 5	$\sim$ 1.5	$\sim$ 0.25
Harvard Pennsylvania Wisconsin	60	10	10	0.75	$\sim$ 0.16
CALTECH	144	16	55	4.5	0.38
Present proposal	275	6	151	5.6	0.55

E) Prototype construction

The construction of a full-scale module of 18 plates as prototype has begun. We expect to assemble this module in the Summer of 1974.

F) Cost

The cost breaks down approximately as follows:

		Per module	Total
Iron	Swiss f.	60,000.-	500,000.-
Scintillator		172,000.-	1,400,000.-
Circuits + phototubes		190,000.-	1,500,000.-
		422,000.-	3,400,000.-

G) Energy resolution and spatial resolution

1. Missing energy

Fortunately a good deal of work[1] has been done on STAC's, both theoretically and experimentally, so that this complex problem is becoming rather better understood. In particular, Engler et al.[2] have measured the performance of a very similar, though smaller, STAC at a number of energies up to 60 GeV. Their result for resolution as function of energy is shown in Fig. 4. The solid curve is an extrapolation according to the linear curve of width versus energy which the authors fit to the data. The dotted curve is the extrapolation according to $1/\sqrt{E}$, which should at least roughly describe the resolution.

To discuss the observed widths, we reproduce in Fig. 5 the data of Engler et al.[2] in which the pulse height distributions observed in a 40 cm × 40 cm × 80 cm STAC for 21 GeV electrons, pions and protons are shown. The magnitude of the signal is 30-35% lower in the case of the hadrons. This "missing energy" itself is no difficulty in principle, since calibrations need to be done anyway. However, the widths of the pulse height distributions for the hadrons are much larger than the ones for the electrons and the origin of the bulk of the hadron width is in the fluctuation of this missing energy. It is therefore important to understand the missing energy. It can be divided into the following categories:

a) "invisible energy" such as nuclear excitation, neutrinos, low energy neutrons, muons that escape, etc.;

b) "saturation" losses due to the fact that slow, heavily ionizing particles produce light with less efficiency than minimum ionizing particles. This effect concerns chiefly nuclear fragments and protons below 10 MeV. In the case of scintillators, the saturation losses are experimentally known;

c) "leakage" energy due to finite detector size. This last contribution clearly depends on the detector dimensions. For our much larger detector it enters into consideration only for the purpose of understanding the effective fiducial volume.

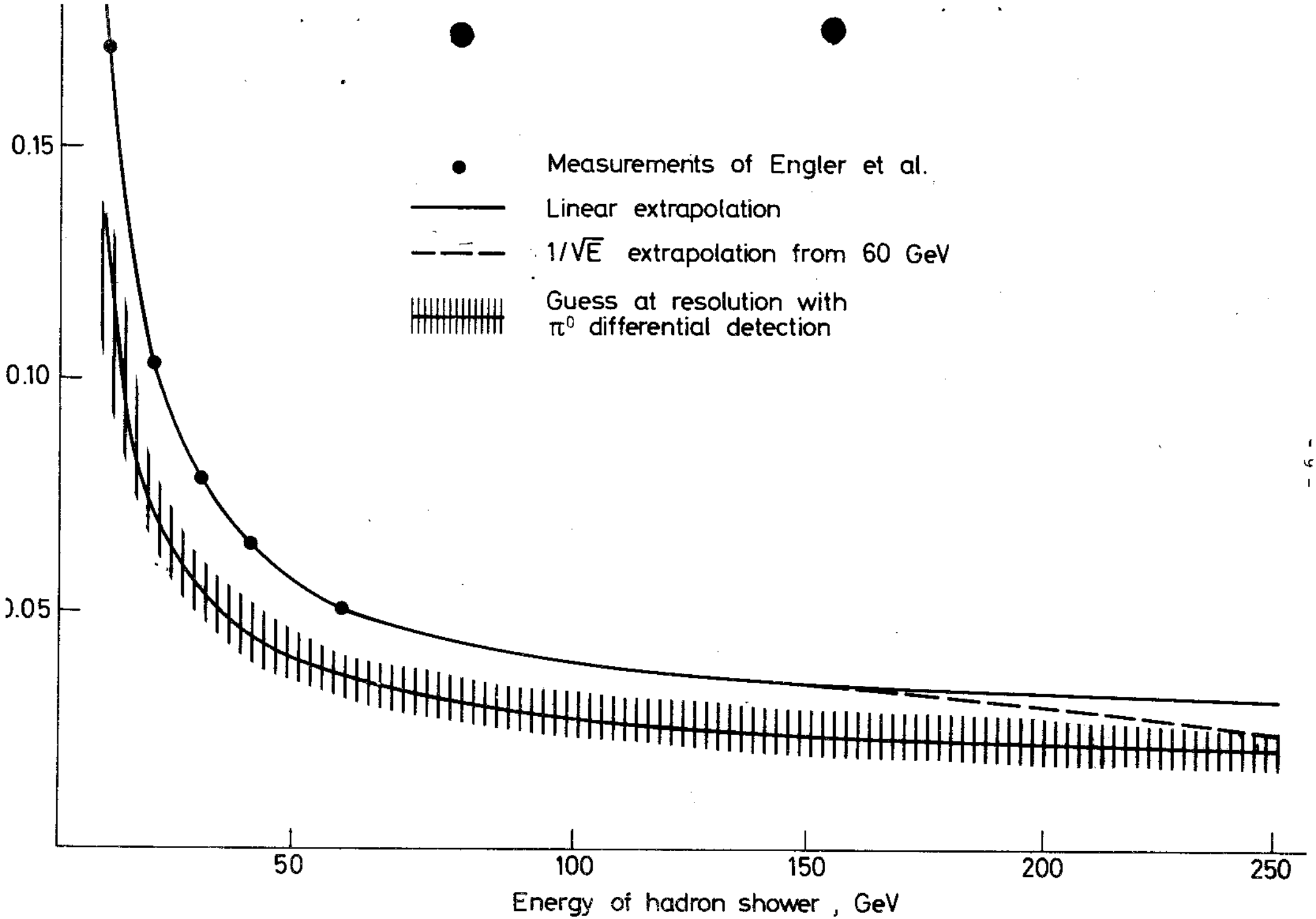

Fig. 4 Energy resolution σ/E of the hadron shower detector

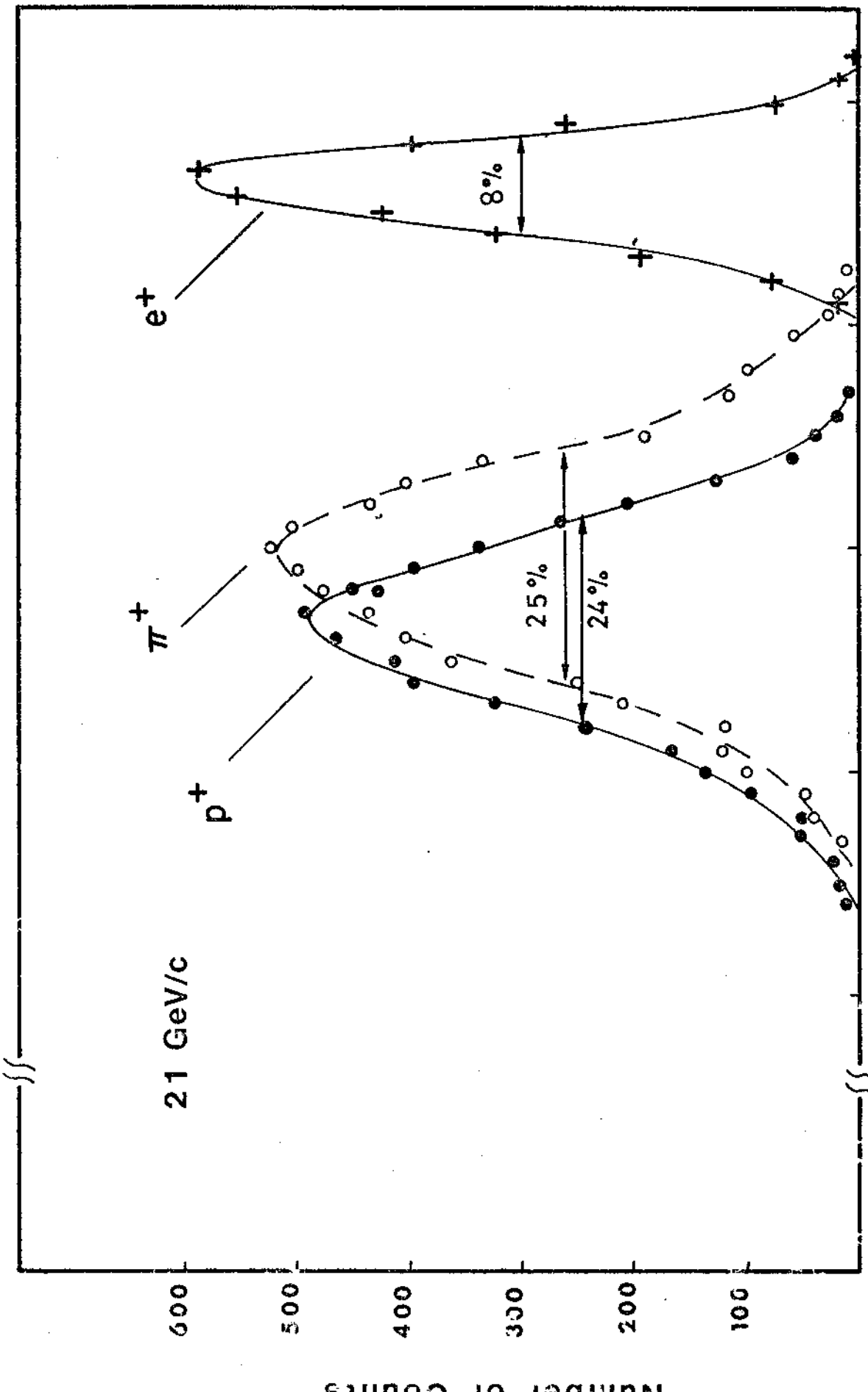

Fig. 5 Pulse height spectra obtained by Engler et al.[2] in an iron scintillator sandwich detector

For the measurements of Engler et al.[2] we understand the three contributions as follows[3]

a)	invisible energy	0.104	(0.115)
b)	saturation loss	0.075	(0.086)
c)	escape	0.13	

Presumably, with a larger detector, within a properly chosen fiducial region, the escape energy will be negligible and the ratio of pulse heights of hadron showers to those of electromagnetic showers will be more near 0.8. The numbers in parantheses are the estimates of the contributions of a) and b) in the case of a detector with no leakage.

The fluctuations produced by this $\sim$ 20% missing energy are two fold:

a) The missing energy occurs in nuclear events, and since there are many fewer nuclear events than plate traversals, the nuclear events will make a larger contribution to the width.

b) Since π^0's give the full energy, fluctuations in the π^0 component contribute to the width.

We estimate the width contribution due to these factors as follows:

a) Fractional width $\gamma = \sigma/E$ due to the fluctuations in the missing energy. This is proportional to the invisible fraction 0.2/0.8 and inversely to the number of nuclear interactions, which is about 1 per GeV. So $\gamma_{\text{Missing Energy}} \simeq 0.25/\sqrt{E}$ (GeV) = 0.025 at 100 GeV hadron energy.

b) Fractional width due to fluctuations in π^0 component. If we take the average π^0 component of the original event as 0.3, and the fluctuations in it to be 40%, independent of energy since the multiplicity is slowly varying with energy,

$$\gamma_{\pi^0} \simeq 0.2 \times 0.12 = 0.024, \quad \text{independent of energy.}$$

The results of Engler et al.[2], $\sigma = 0.051$ at 60 GeV, can be understood in terms of these contributions (4%) and a contribution due to fluctuations in leakage.

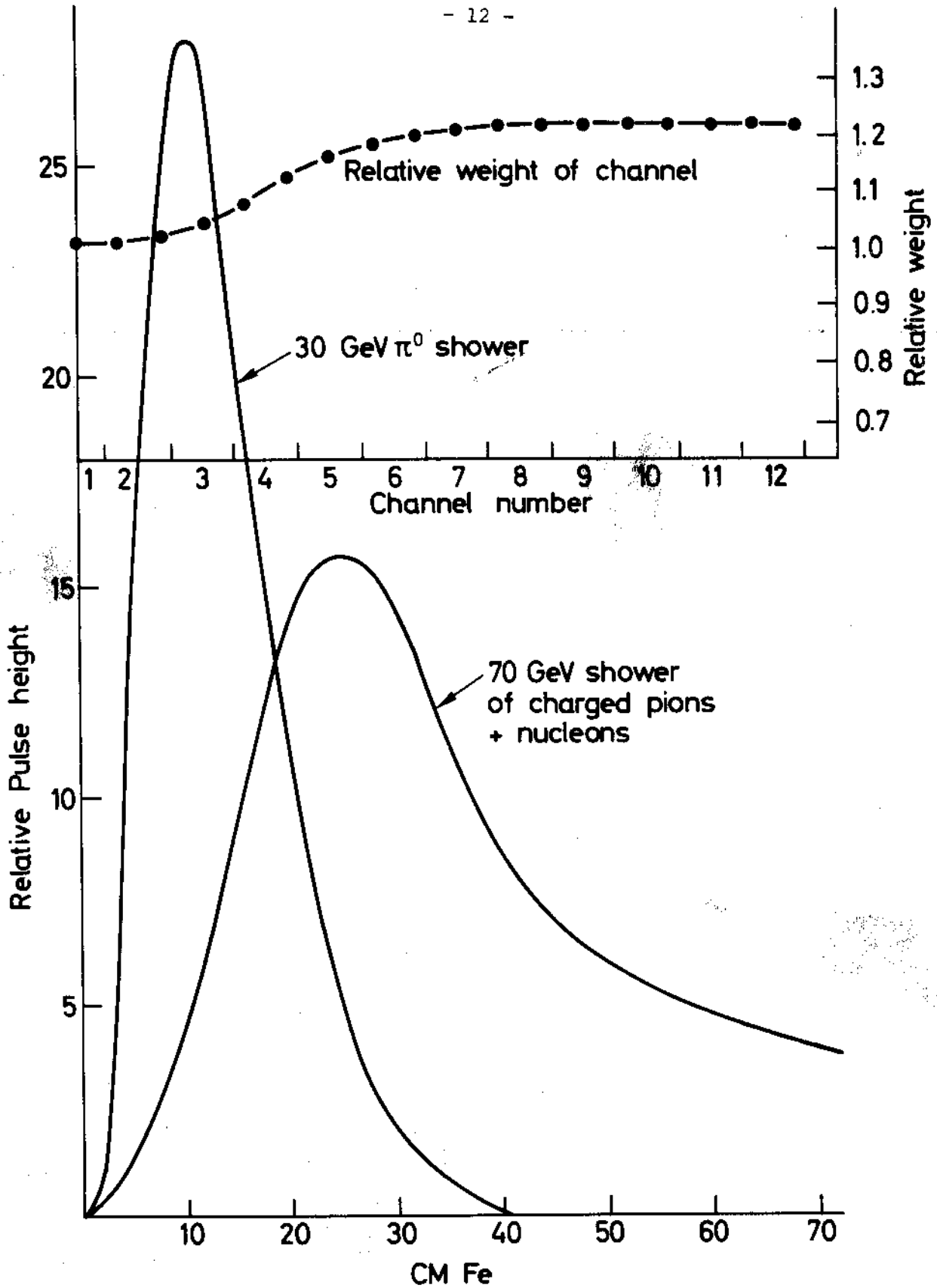

Fig. 6 Differential π^0-detection. The figure shows the longitudinal developments of electromagnetic and hadronic showers. The insert gives a weight function. A detector response independent of the initial π^0-content of a hadron shower can be obtained by giving a smaller weight to the beginning of a shower development (see text).

2. π^0 differential detection

The electromagnetic shower develops in the iron much more quickly than the hadronic shower. The originally produced π^0 component can therefore be differentiated if the detector resolution in the beam direction is adequate. It is for this reason that we have chosen to combine only two scintillators into one pulse height channel. The method is illustrated in Fig. 6 with a typical shower, 30% π^0 component, 70% hadron component. The early pulse height channels in the region of E.M. shower development are weighted less than the subsequent channels according to the relative contribution of the two components. If the same recipe is then applied to showers with different relative π^0 component, the fluctuation is much reduced with respect to the fluctuation in the usual case of uniform weight, so that the fluctuations due to this effect are reduced to a level of 1% or below.

3. Effect of sampling thickness

In Section G.1 the fluctuation problem was discussed in detail, showing that the resolution is dominated by nuclear processes. These have a mean-free path of $\sim$ 15 cm in iron. As long as the sampling thickness is much inferior to 15 cm, the sampling can be expected to have only a small effect on the resolution. We expect, therefore, that the 3 cm we have chosen is practically equivalent to zero thickness [4]. This is shown experimentally by the result of Turkot et al.[5] who find no measurable difference in STAC's of 1.25 cm and 2.5 cm plate thickness, and Engler et al.[6] who find a 10% improvement in going from 4 cm to 2 cm plates *). These measurements confirm that the contribution to the resolution of a sampling thickness of 3 cm is small.

---

*) These are the only results presently available in which different sampling thicknesses in the range of a few centimetres are compared in the same apparatus. We refrained from combining data-points obtained in different experimental set-ups since the systematic deviations cannot be evaluated.

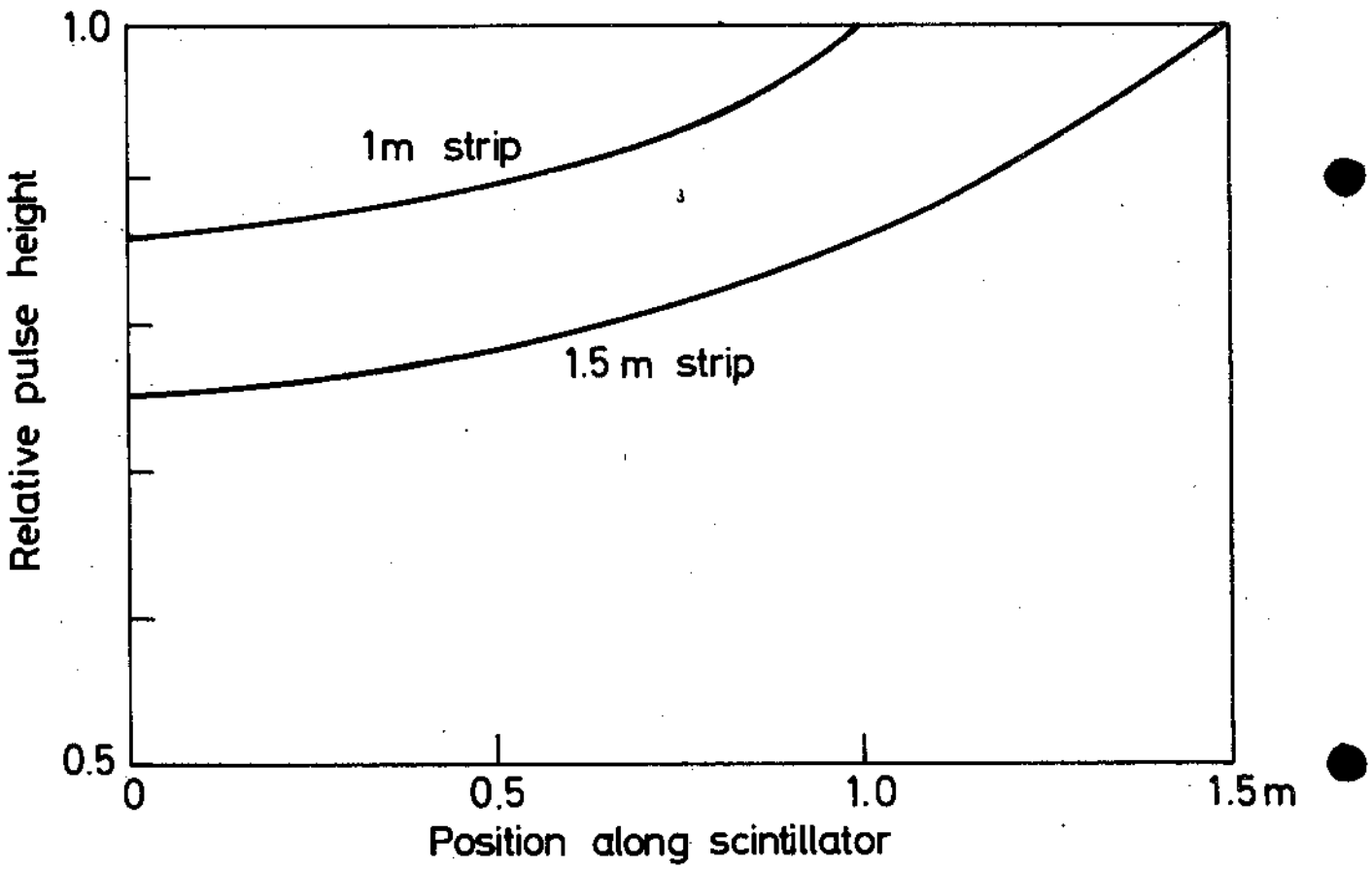

Fig. 7 Light attenuation in scintillators as used in the hadron shower detector

4. Effect of light attenuation in scintillator on resolution

The pulse height distribution for a scintillator of the type and geometry we are using is shown in Fig. 7. For the worst case (1.5 m lengths) this corresponds to maximum variation - outside edge to inside edge - of a factor 4/3. This must be corrected with the help of the nearby counters rotated through 60 and 120°. Since we measure the position of the shower easily to 3 cm, the contribution to the width introduced by this attenuation will be of the order of $\frac{1}{3} \times \frac{3}{150} = \pm 0.007$. This is much less than the fluctuation widths and therefore does not effect the resolution.

5. Total width

Following these arguments, a STAC as we propose, using differential π^0 detection, may be expected to have a resolution σ varying from $\sim$ 4% at 50 GeV to $\sim$ 2% at 200 GeV. How well one will achieve this excellent resolution permitted by the physics of the detector will depend upon how well one does the electronics, the calibrations and the programming.

H. Calibration and monitoring

The monitoring of the 2880 channels and 5760 phototubes will be performed with light diodes, cross-checked by means of the pulses from the minimum ionizing muons. Calibration by high-energy electrons, pions and protons will require the bubble chamber hadron beam. Provisions for steering this beam to the centre of the detector are essential.

III. HEAVY TARGET AND MUON SPECTROMETER

A) Magnet design

The heavy target muon spectrometer design remains unchanged from the original proposal. The mechanical design of the magnet units has been completed (Fig. 8), and field studies on a 1:10 scale model show that the average field at 10 kW per module will be 16.5 KG.

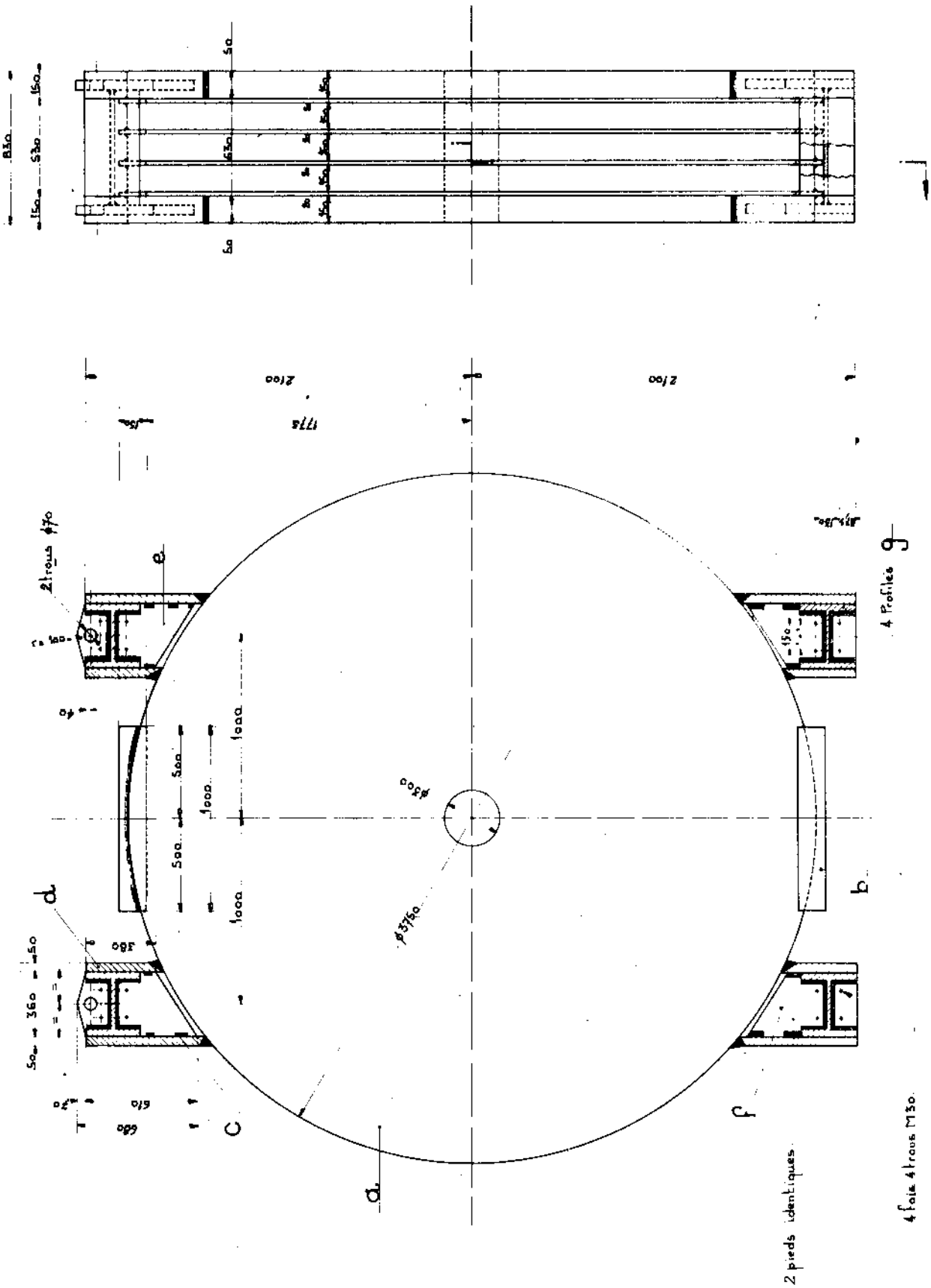

Fig. 8 A module of the muon spectrometer

B) Drift chamber design

Drift chamber design is going ahead at Saclay, following the simple design developed at Harvard[7]. A full-scale model with three sets of wires at 60° to each other is under construction. The shape of the external frame is hexagonal, with the ground plates made of aluminium honeycomb plates, which are light and stiff. The thickness of these plates is 2 cm each (weight $\sim$ 100 kg) and they are rigid enough to make stiffeners inside the useful area of the chamber unnecessary. The distance between two sense wires is 6 cm and the ground planes are 3 cm apart. Each wire set is parallel to one side of the hexagon. Details of the wire mounting and support frame are shown in Fig. 9.

C) Momentum resolution

The solid angle of acceptance for muons produced in the hadron shower detector is a function of the number of units traversed and so of the momentum resolution. The latter is dominated by the multiple scattering even at the highest momenta, provided a resolution of 1 mm is achieved in the drift chambers. Molière- and single scattering contribute to the scattering of the muons in the iron core magnet only to less than 10^{-5}. The angular distribution is therefore Gaussian down to this level. The momentum resolution $\Delta p/p$ as function of the number of units traversed is shown in Fig. 10. The solid angle varies from 0.18 sterad (θ = 240 mrad) for three units with $\Delta p/p = 0.15$, to 0.013 sterad (θ = 75 mrad) for 24 units with resolution $\Delta p/p = 0.053$.

D) Solid angle for muon detection

The solid angle available for muon detection will be most important for the investigation of the q^2 - ν plot, particularly at high q^2 and ν. In Fig. 11 and Fig. 12 the acceptance in the centre-of-mass production angle and in q^2 are respectively shown as a function of the incident neutrino energy. For acceptance we have taken as definition the acceptance for those processes which will be detected in the spectrometer if they occur in the centre of the fiducial volume of the hadron shower detector.

In Table II we compare the acceptance of our muon spectrometer with those at present at NAL.

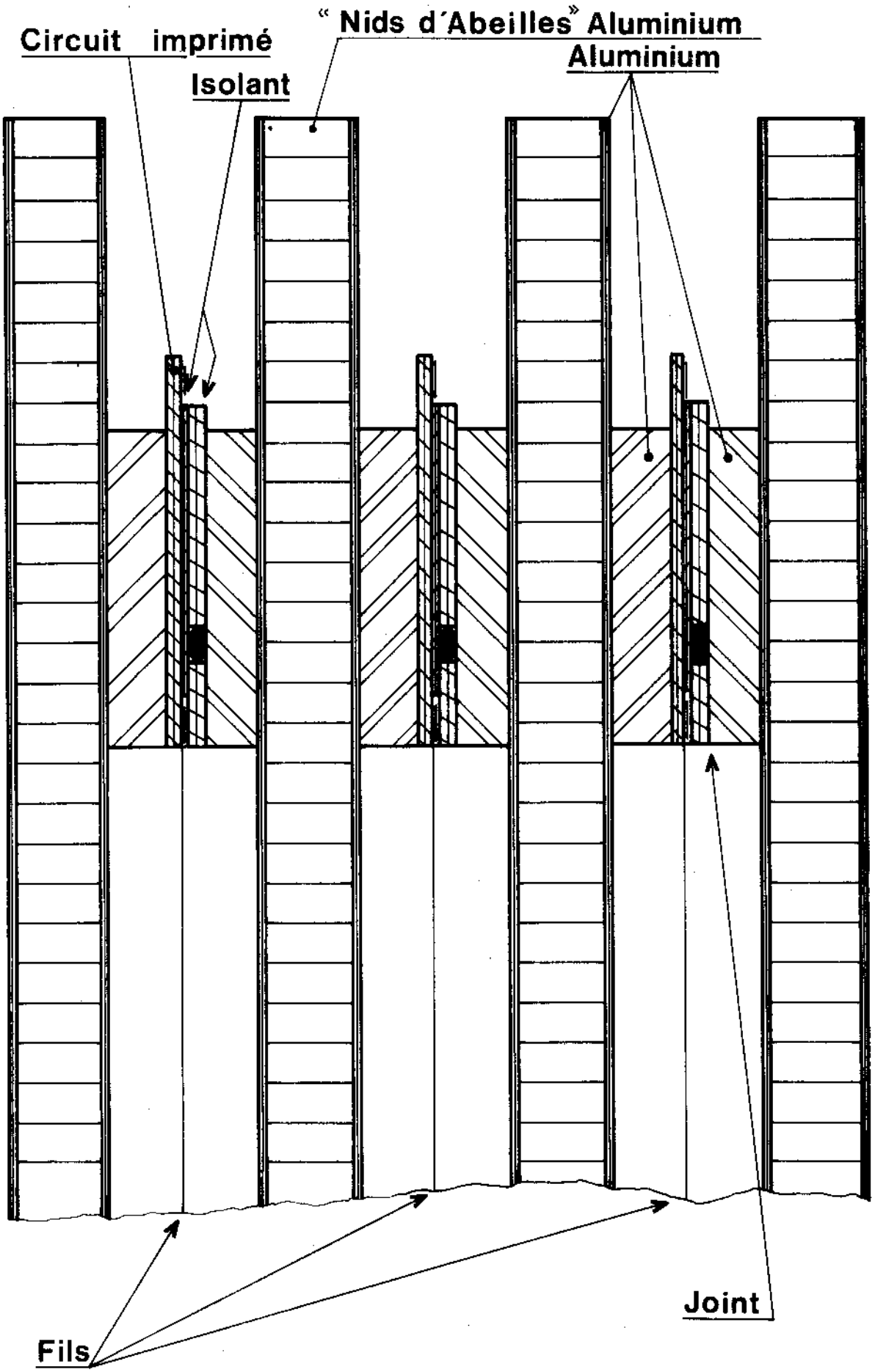

Fig. 9 Detail of the drift chamber design

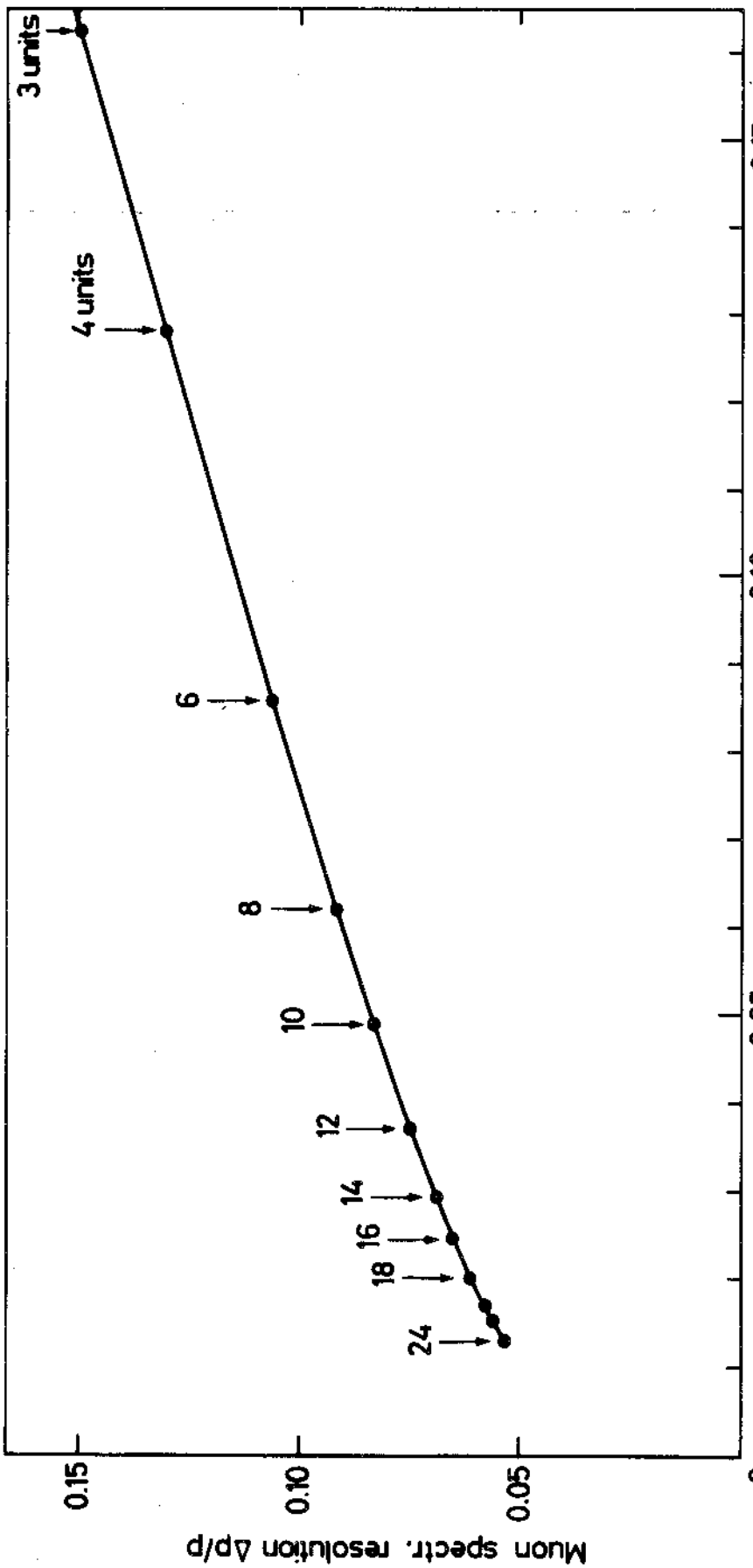

Fig. 10 Momentum resolution in the muon spectrometer as a function of the solid angle available to muons produced in the centre of the hadron shower detector.

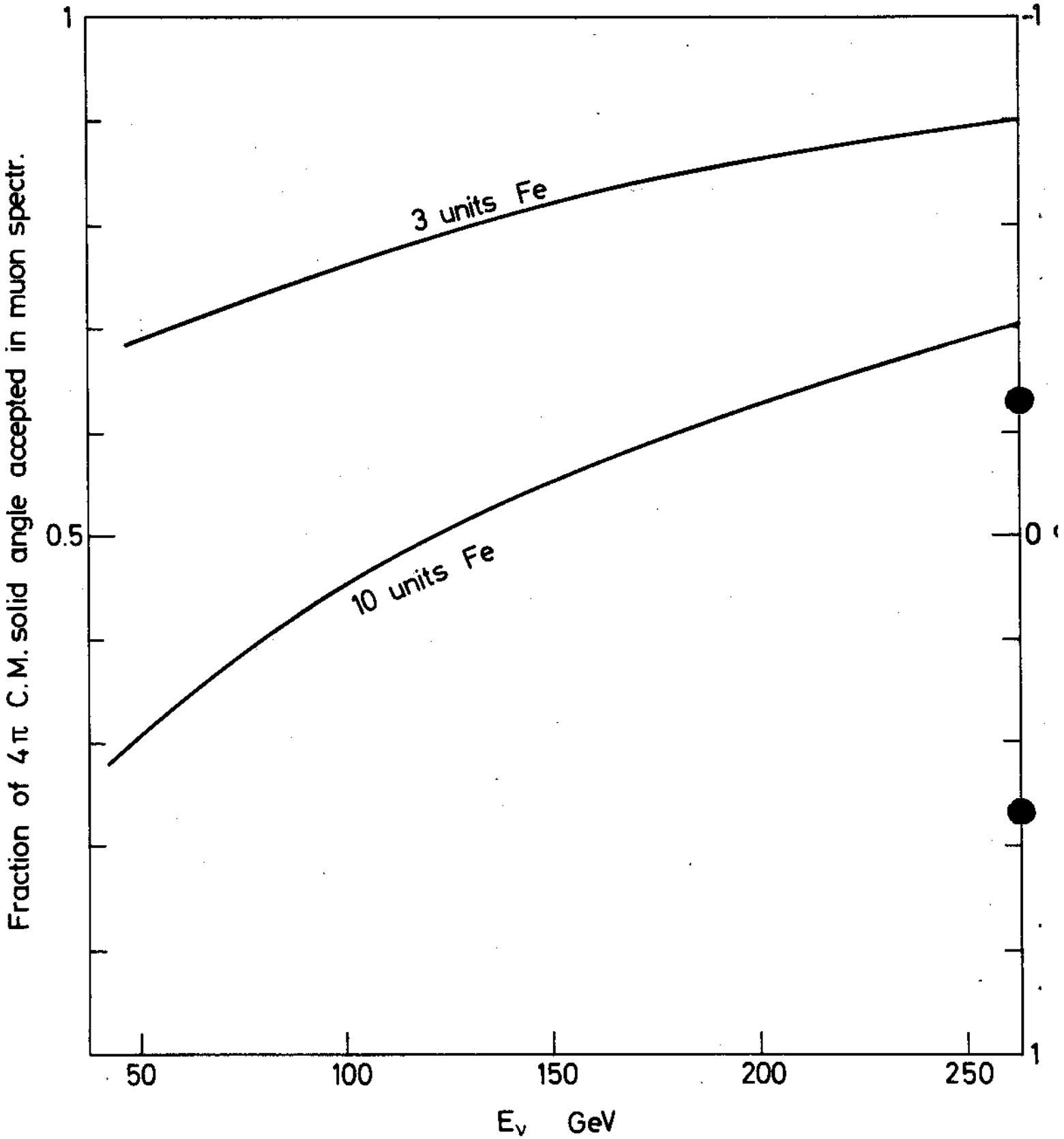

Fig. 11 Average acceptance of the muon spectrometer as a function of the centre-of-mass production angle.

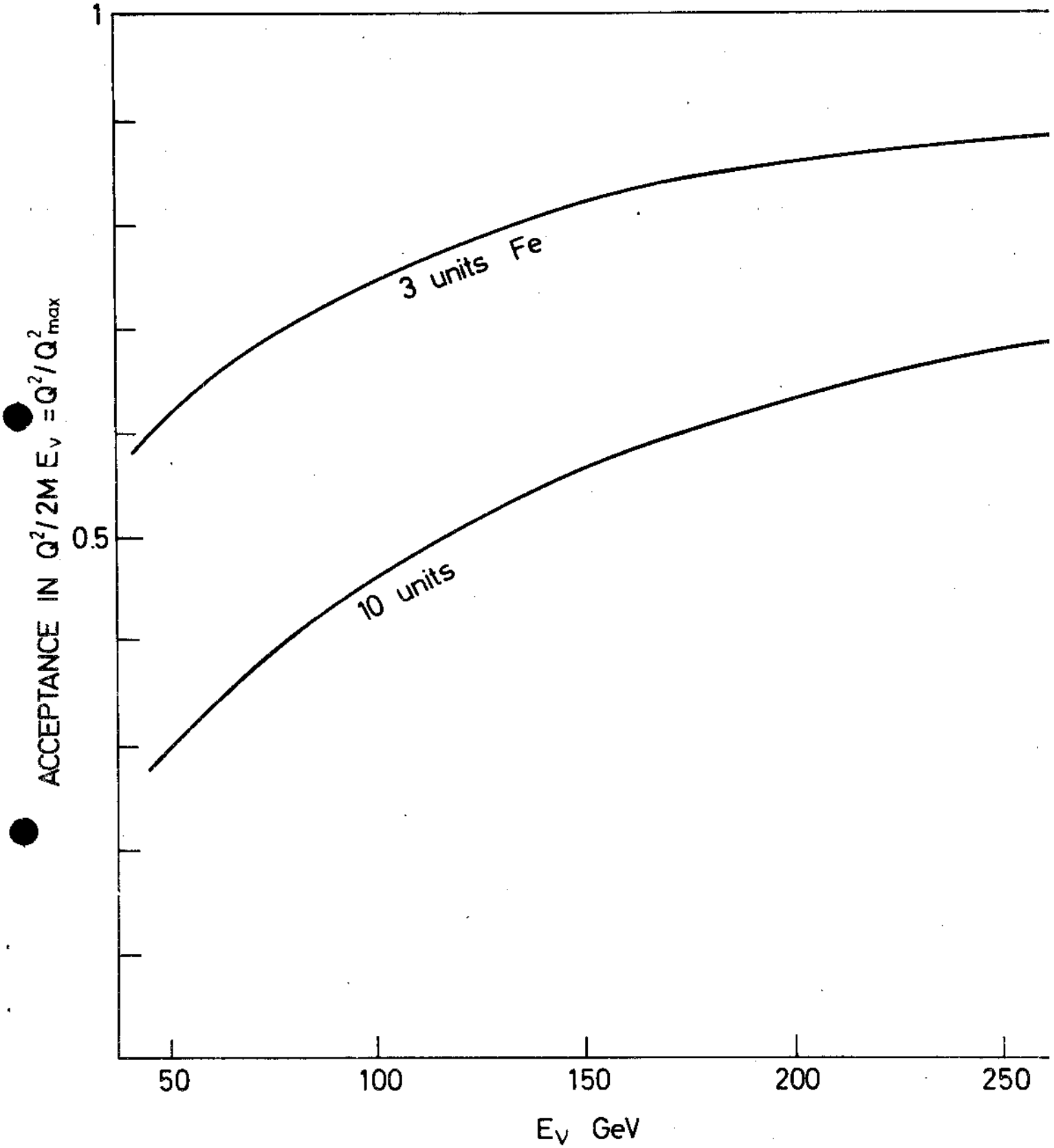

Fig. 12 Average acceptance in Q^2 of the muon spectrometer.

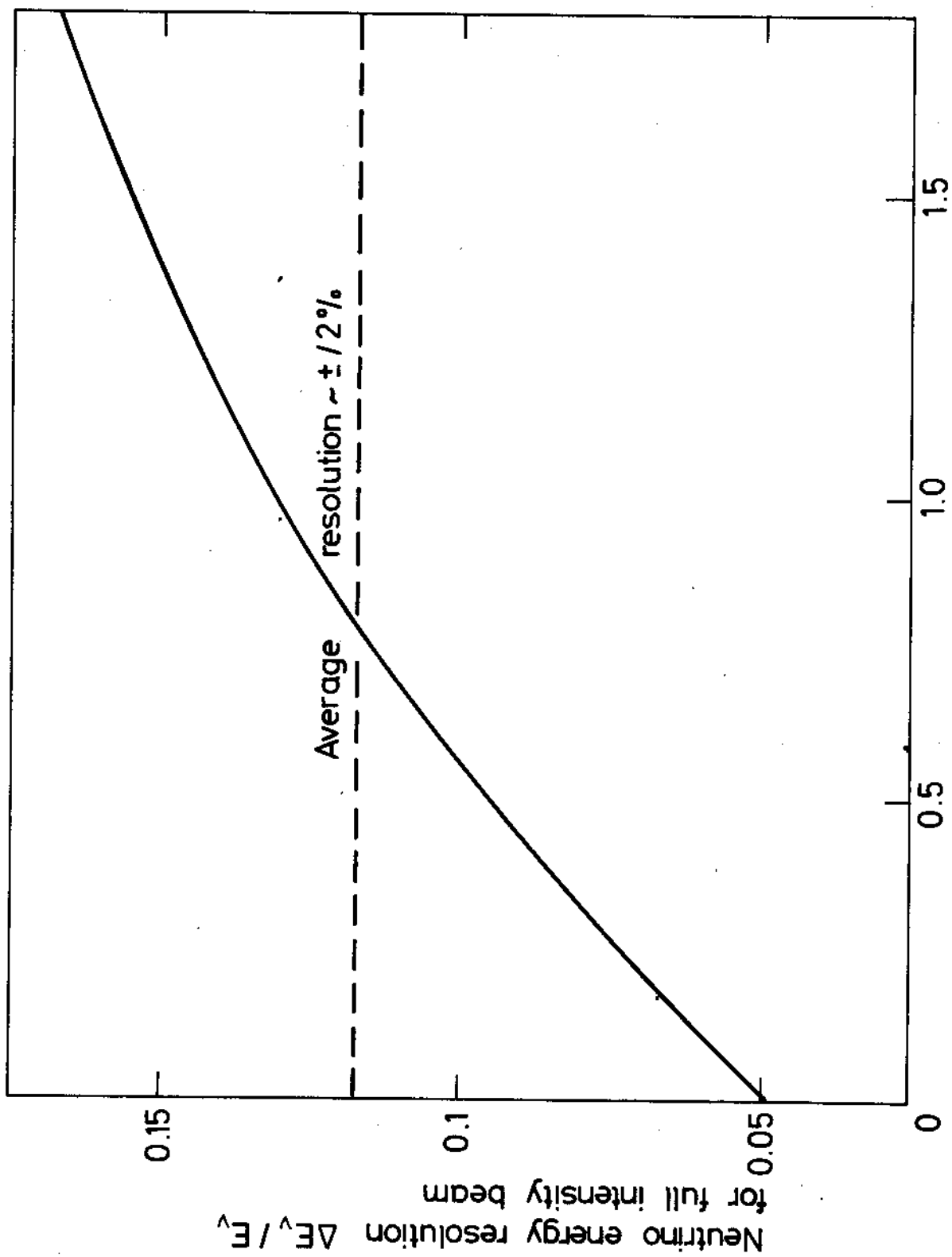

Fig. 13 Neutrino energy resolution in the narrow band beam as a function of the radial position of an interaction

Table II

Solid-angle acceptance $\Delta\Omega$ and resolution $\Delta p/p$ of spectrometers at present at NAL and of this spectrometer for different numbers of iron core magnets

Experiment	$\Delta\Omega$	$\Delta p/p$
Harvard Pennsylvania Wisconsin	0.05	± 10%
CALTECH	0.017	± 14%
Present proposal	0.013	± 5.3%
	0.05	± 8.2%
	0.18	±15%

E) Big target

The iron of the magnet acts also as a 1400 ton target which will be important in the study of rare processes involving muons and not requiring good hadron shower measurement. Examples of such processes are the reaction $\nu_\mu + e^- \rightarrow \mu^- + \nu_e$, intermediate boson production with subsequent muonic decay, heavy lepton production with decay to the "wrong" charge muon, and "trident" production: $\nu_\mu + Z \rightarrow \nu_\mu + \mu^- + \mu^+ + Z$ as discussed in Section V.

IV. WEST AREA NEUTRINO BEAMS AND EXPERIMENTAL INSTALLATIONS

An excellent realization of the narrow band beam has been studied for the West Area[8], and its design is practically completed. It can accept a primary charged beam of up to 275 GeV, and is designed for maximum acceptance and minimum angular divergence. If the radial position of the neutrino interaction is measured, the neutrino energy will be known with the precision shown in Fig. 13. The average uncertainty over the fiducial area of the detector is 12%.

It is possible to improve this resolution with consequent loss in intensity by decreasing the decay length and the momentum acceptance. A factor two improvement in resolution produces a factor five loss in intensity. We therefore expect to use almost exclusively the full intensity version of the narrow-band beam. We will also make use of the wide band beam as soon as a spill time of 2 msec is available (see Section V).

As we have made clear from the beginning, we consider the West Area the logical place for this experiment. Probably the position immediately behind BEBC is best, since it makes it possible to steer the BEBC hadron beam into the detector for calibration which is essential. If it is possible to have this beam also in front of BEBC, this would be an even better location.

We wish to call attention to the fact that it is important that the installation facilities be ready at the end of 1975 or, at the latest, at the very beginning of 1976 if the apparatus is to be assembled and tested to be ready for the Summer of 1976.

V. EXPERIMENTAL PROGRAMME

A) Measurement of the inclusive neutrino cross-section in iron

The determination of the structure in the Q^2-ν plot aims at the following chief topics:

- test of scaling up to very high Q^2
- search for W propagator effects
- separation of the three independent structure functions
- search for effects due to new particle production (i.e. vector boson, charmed particles, etc.).

By far the most exciting possibility, we feel, is that of seeing the breakdown of scaling due to the effects of the intermediate boson propagator. The mass of the intermediate boson expected on simple arguments of the correspondence of the electromagnetic and weak interactions is $\sim$ 30-40 GeV. We believe that these arguments, if not compelling, are very attractive, and that there is a real likelihood that the intermediate boson of this

mass exists. The search for its propagator effect seems to us, therefore, the most important aim of the CERN neutrino programme.

This is a very difficult experiment, requiring extensive, systematically good data at high Q^2, in a region of low event rate. It is therefore also highly likely that the experiments at NAL will not yet have accumulated adequate data, and that the second generation experiments at CERN can still make the vital contribution. Our apparatus, with good and uniform coverage of the high Q^2 region, is well suited to studying this propagator effect.

The measurement errors in the Q^2-ν plot are shown in Fig. 14. The measurement errors are well under control and the small systematic uncertainty will allow the separation of the effect of the boson propagator from other possible sources of non-scaling.

In the lower half of the Q^2-ν plot the errors in Q^2 are mainly due to the error of the muon angle determination caused by multiple scattering in at least one metre of iron necessary to stop the hadron shower. For larger Q^2 the error is dominated by the error in the muon momentum. Also here the multiple scattering in the iron, which is well understood, determines the measurement accuracy. The resolution in ν is given by the energy resolution of the hadron calorimeter; the systematic error is largely determined by the calibration procedure. It should be noted that the effect of the Fermi motion naturally sets the limit to observable finer structures in the Q^2-ν plot and not the measurement accuracy.

B) Hydrogen and deuterium targets

For a complete study of inclusive neutrino interactions, the use of elementary targets is essential. In our proposal we have given a possible experimental layout for such an exposure (Fig. 7 of the proposal). Since both our calorimeter and the muon spectrometer are modular we can measure the Q^2-ν plot in H_2 and D_2 simultaneously in an identical set-up. Such an exposure can be performed in a second stage of the experiment when the calorimeter has been calibrated in the narrow band beam and a wide band beam with sufficient spill time ($\geq$ 2 msec) will be available.

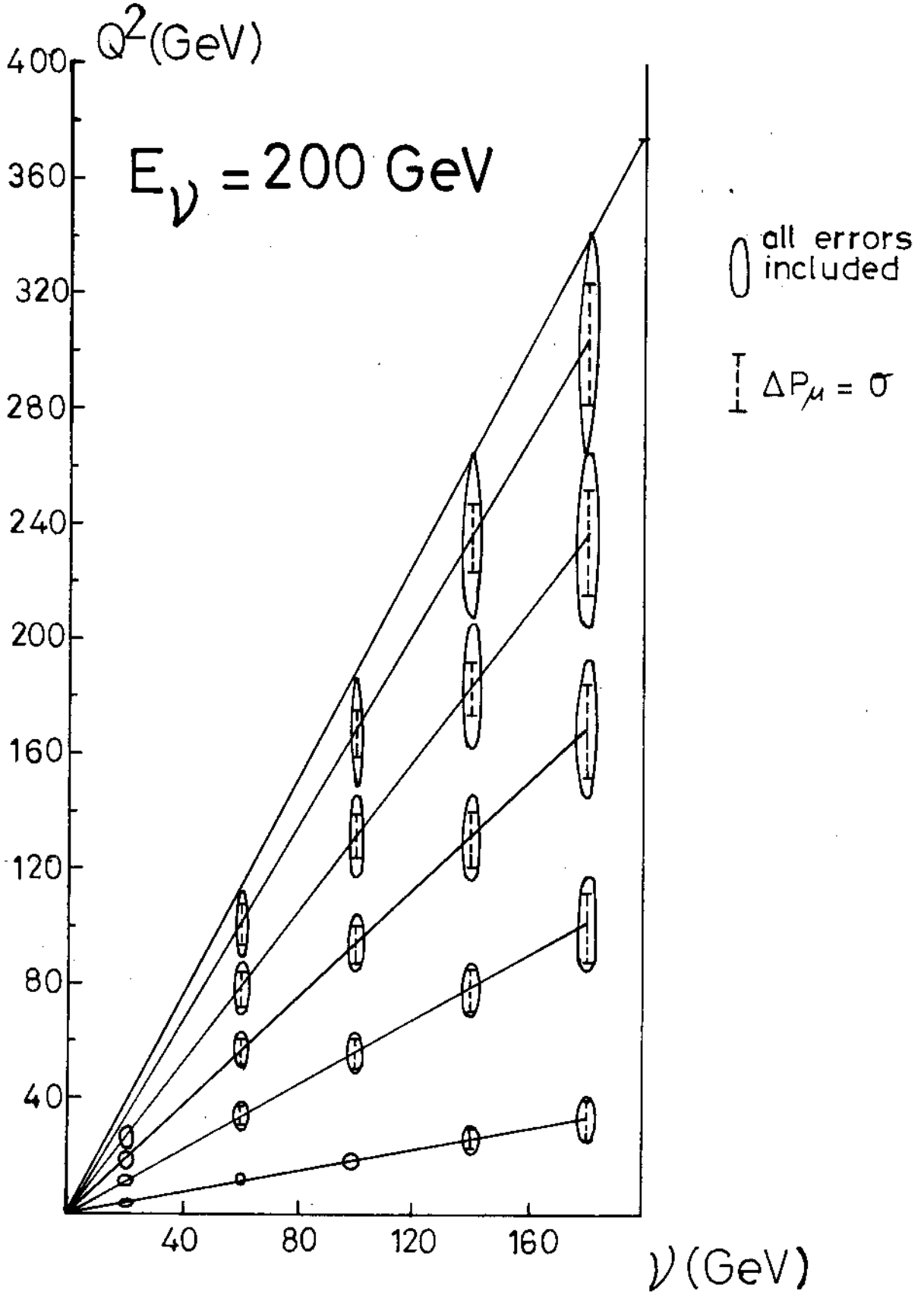

Fig. 14 Measurement errors in the Q^2-ν plot

The main interest will be in events with large neutrino energies (E_ν > 50 GeV) where bubble chambers are of limited use. The advantages of this set-up are:

- measurement of the total hadronic energy;
- clean muon identification and measurement;
- good acceptance in the Q^2-ν plot for E_ν > 50 GeV;
- large event rates compared with BEBC: we expect $\sim$ 0.4 events/burst in H_2 (2 tanks) and 0.45 events/burst in D_2 with E_ν > 50 GeV at 10^{13} ppp;
- the relative normalization between H_2 and D_2 is naturally given, thus allowing an immediate evaluation of differences in the νn and νp differential cross-sections.

C) Rare processes

For the search of rare processes, "strange muons", the whole mass of the magnetic spectrometer can serve as a target in addition to the calorimeter and yield event rates which cannot be achieved by other proposed detectors. The magnets represent a mass of 1560 t out of which 1400 t are useful for this purpose.

1) Search for the diagonal leptonic interaction and measurement of its coupling constant G. The reaction $\nu_\mu + Fe \rightarrow \nu_\mu + \mu^- + \mu^+ + Fe$, i.e. the coherent trident production in the Coulomb field, has a cross-section of the order of $\sigma \sim Z^2 \cdot \alpha^2 \cdot G^2 \cdot E_\nu \cdot \log E_\nu$. In the conventional V-A theory $G = G_F$ is the Fermi coupling constant. However, the coupling constant for the "diagonal" interaction has never been measured and could well be substantially different from G_F [9].

In a wide band beam assuming V-A coupling, one can expect about 200 events originating in the magnets and 40 events originating in the calorimeter for a run of 10^{18} interacting protons. The corresponding event number in Gargamelle is quoted to be 2 events[10]. We expect the background from multipion production and single π production to be under control for the events from the calorimeter and tolerable for the ones from the magnets, if the spectrometer is partially equipped with scintillator.

2) Search for the W^+ via its leptonic decay mode

The $W^+ \to \mu^+\nu$ decay will produce μ^+'s having a peak in the transverse momentum at $m_W/2$, which is a unique feature. Together with the μ^- coming from the production reaction $\nu_\mu + N \to \mu^- + W^+ + N^*$ it will form a dimuon event with a signature which is completely different to that of trident events. Using the production cross-sections of Brown and Smith[11], a branching ratio $\Gamma(W^+ \to \mu^+\nu)/\Gamma(W^+ \to \text{all}) = 0.3$ and a cut $p_\perp > 0.3\ m_W$, our sensitivity is estimated to be sufficient to see 200 events in a run of 10^{18} protons in the wide band beam if the W^+ has 15 GeV mass.

3) Study of the inverse μ decay

The reaction $\nu_\mu + e^- \to \mu^- + \nu_e$ offers the possibility to measure the quantity $\lambda = 2\ \text{Re}\ (g_V g_A)/(|g_V|^2 + |g_A|^2)$.

The cross-section for this reaction is $\sigma(\nu_\mu e^- \to \mu^- \nu_e) = 1.6\ E_\nu\ (\text{GeV})\, 10^{-41}\ \text{cm}^2$. Again, in a narrow band beam we expect $\sim$ 200 events, about 20 times the rate for Gargamelle and 100 times the one in BEBC filled with hydrogen.

The background comes from the reaction $\nu_\mu n \to \mu^- p$ where the proton is not seen. This reaction has a cross-section of $0.7 \times 10^{-38}\ \text{cm}^2$ independent of neutrino energy. The kinematics of the leptonic process is sufficiently different so that we can expect the reaction to be identifiable in the larger part of the kinematical region.

4) Search for heavy leptons

Existence of heavy leptons M^+ belonging to a triplet (M^+, μ^-, ν_μ) is required by some of the unified theories of weak and electromagnetic interactions. The signature of such events would be the presence of a μ^+ from the decay $M^+ \to \mu^+\nu_\mu\bar{\nu}_\mu$ and the absence of a μ^-, i.e. an apparent failure of lepton number conservation. Production cross-sections from the parton model[12] using the structure functions from e-d scattering, yield rates in a narrow-band beam such that heavy leptons with mass up to 15 GeV can be detected. The low $\bar{\nu}$ contamination of the narrow-band beam (10^{-4}) is required to keep μ^+ background below 5%. Background from multipion production with subsequent $\pi \to \mu^+\nu$ decay and missing the μ^- is even smaller.

REFERENCES

1) We are very indebted to Profs. Engler, Sciully, Selove and Willis for making unpublished material available to us.

2) "Results of test measurements of a STAC at Serpukhov, Karlsruhe/CERN-ITEP Collaboration, preliminary report.

3) These estimates are based on detailed calculations performed by T.A. Gabriel at Oak Ridge National Lab. for Prof. W. Willis. We wish to thank Prof. Willis for making the calculations available to us.

4) B.C. Barish et al.: Calibration of a sampling total absorption detector at 200 GeV, California Inst. of Tech.-NAL Collaboration, preliminary report, September 1973.

5) F. Turkot et al., Performance of a sampling calorimeter at 3 to 17 GeV, BNL-Pennsylvania-Wisconsin Collaboration; University of Pennsylvania, Internal report, October 15, 1973.

6) J. Engler, W. Flauger, B. Gibbard, F. Mönnig, K. Runge and H. Schopper, Nucl.Instr. and Methods, 106, 189-200 (1973).

7) D.C. Cheng, W.A. Kozanecki, R.L. Piccioni, C. Rubbia, L.R. Sulak, H.J. Weedon, and J. Wittaker, Very large proportional drift chambers with high spatial and time resolution, Harvard University preprint, submitted to the Int.Conf. on Instrumentation for High-Energy Physics, Frascati (1973).

8) J.V. Allaby et al., West Area Neutrino Facility (WANF), CERN/SPSC/T 73-7 17 September 1973.

9) M. Gell-Mann, M. Goldberger, V. Kroll and F.E. Low, Phys. Rev. 179, 1518 (1969).

10) CERN/ECFA/72-4, Vol. I, p.82.

11) R.W. Brown and J. Smith, Phys. Rev. D3, 207 (1971).

12) J.D. Bjorken and C.H. Llewellyn-Smith, Phys. Rev. D7, 887 (1973).

APPENDIX

COMPARISON OF DIFFERENT TECHNIQUES

Recently, proposal SPSC/P 73-3 has appeared with a partially overlapping physics programme, but with a rather different technical realization of the apparatus. The hadron calorimeter employs liquid argon instead of the scintillator to sample the hadron shower development; an air core magnet is proposed in contrast to our iron core magnets for the muon spectrometer. We therefore consider it important to bring some comparisons of the capabilities of the two apparatuses.

A. Comparison of hadron shower detectors

1. Resolution

Although substantial data on resolution exist in the scintillator case, no data exist on the resolution of hadronic showers in argon. However, the fundamental limitations are very similar. We have seen in Section G that these are due to fluctuations in the "missing" energy. This was divided into two parts: "invisible", $\sim$ 57%, and "saturation", $\sim$ 43%. The invisible part is the larger, and the same for both detectors. The saturation part is due to different mechanisms in the two cases. It has been extensively studied for scintillators, but hardly at all as yet in the case of liquid argon. The saturation effect certainly exists here also and we have no reason to expect that it will turn out to be substantially less than in the scintillator case*).

We have also seen that the sampling thickness is not important, as long as it is thin compared to 15 cm, so that the thin plates which are

---

*) In SPSC/P 73-3 two sets of experimental data were presented which were interpreted by the authors as showing that the missing energy is not missing in argon. We do not succeed in following these data to that conclusion. In the same paper there is a measurement of this effect attributed to Willis without further reference. We cannot verify this reference.

convenient for liquid argon give no especial advantage. The fundamental limitations are therefore not different for the case of the two methods, and, as we have seen, permit excellent resolution in the 100 GeV range.

We feel further that the experience accumulated in pulse height work with scintillators makes it reasonably sure that the resolution can, in fact, be achieved.

2. Geometry - density

The average density enters into the design in three ways, all favouring high density. One is the total weight of detector required to achieve a given fiducial weight, another is in the size of the magnet required to achieve a given solid angle for muon detection, and a third is the muon background due to π-μ and K-μ decays. This consideration strongly favours the scintillator.

The average density of our detector is 5.6, including the space required for the two drift chambers. In the case of the argon detector proposed in SPSC/P 73-3, the density of the lattice itself is 4.6, already considerably less, and is further reduced to $\sim$ 3.6 by the requirement of packaging and space for drift chambers. If one wishes to leave a lateral space of 120 g/cm^2 for the shower development, and wishes to be able to have uniform detection for hadron emission angles up to 100 mrad, both rather minimal requirements, the effective fiducial area is reduced from 7.8 sq.m. to 5.6 sq.m. in the scintillator case, and from 9 sq.m. to 5 sq.m. in the argon case.

Another geometrical disadvantage of the liquid argon detector in a modular construction such as has been proposed has to do with the "dead regions". These are the ends and beginnings of the tanks and include one half of the first + last plate, the liquid to the container walls and the container walls themselves. No constructional details are provided but if the total dead region is equivalent, for instance, to 5 cm of iron, this will cause differences of $\sim$ 10% between the energies observed for showers centred on these "dead regions" and showers well contained within the tank. This can, in part, be corrected by proper programming, but it is unpleasant and increases the width.

3. Construction

In the case of the scintillator, this is simple. The plates are welded into a self-supporting structure. The scintillators are purchased and are standard. The light-guides are moulded. A module is rigid and weighs 35 tons. To turn the apparatus on or off, it is only necessary to turn switches.

In the case of the argon, the design and construction of cryogenic tanks with acceptable dead space and dead weight, with proper access, cryogenics and storage seemed to us time-consuming in design, construction and testing, as well as expensive. In the absence of a proposed mechanical design it is difficult to judge the validity of this opinion.

4. Conclusion

Both devices are capable of excellent energy resolution; however, the good density and geometrical properties of the scintillator sandwich, simplicity of design and construction and very probable substantially lower cost and construction delays makes us believe that the scintillator sandwich is the better choice if one wants to get the best possible physics started as early as possible at the SPS.

B. Heavy target and muon spectrometer

Before we start to make a detailed comparison, we would like to call attention to the obvious advantages of an iron core magnet:

1) very large target weight offers unique possibility for some kinds of rare events;

2) large solid-angle and consequently larger acceptance in the Q^2-ν plot;

3) resolution independent of achieving specially high precision in the wire chambers;

4) resolution equally good at high and low momenta;

5) design and construction simplicity;

6) relatively low cost; and

7) very little power consumption.

1. Momentum resolution

In Section III we discussed the momentum resolution of the iron core magnet as a function of the number of units traversed or equivalently as a function of the solid angle available. For a comparison, 10 units of iron core magnet subtend the same solid angle as the air core magnet, namely 0.05 sterad (θ = 125 mrad).

The resolution of the air core magnet depends on the momentum, and on the spatial resolution which can be achieved in the drift chambers. In Fig. 15 we show the resolution which is obtained with the ten iron core magnets (8%) with that which can be expected with the air core magnet as a function of the energy, for three different values of the measurement resolution in the drift chambers: 0.3 mm, 0.5 mm and 1 mm. In obtaining these results we have averaged over a 4 m horizontal aperture, assuming that the chambers in the field will work, and the normal conductor version of the magnet. Our own opinion is that a resolution of 1 mm for this size of chamber is about what can be expected.

2. Solid angle for muon detection

The dense packaging of our hadron shower detector and of the muon spectrometer results in an appreciable increase of the solid angle available for the measurement of the muons as compared to the case of an air core magnet. As already pointed out, the solid angle of the air core magnet for an event taking place in the centre of the shower detector is 0.05 sterad, whereas in the case of the iron core magnet the solid angle can be as large as 0.18 sterad with still acceptable momentum resolution. This is particularly important in the study of the Q^2-ν plot at large Q^2. Large Q^2 corresponds to backward angles in the centre-of-mass and to correspondingly large laboratory angles. This can be seen in Figs. 11 and 12 where the acceptance of our apparatus is shown in c.m. angle and Q^2. The acceptance of the proposed air core magnet is given by the curves labelled "10 units". For high Q^2 events 3 units give a satisfactory momentum measurement, therefore the acceptance of the spectrometer we are proposing is very much superior in the high Q^2 region. This is also shown in Fig. 16. This high Q^2 region is the region which is relevant to the search for the propagator effects of the intermediate boson. Since this effect is small, it is important to have not only good acceptance in this region, but also uniform acceptance for systematic reasons.

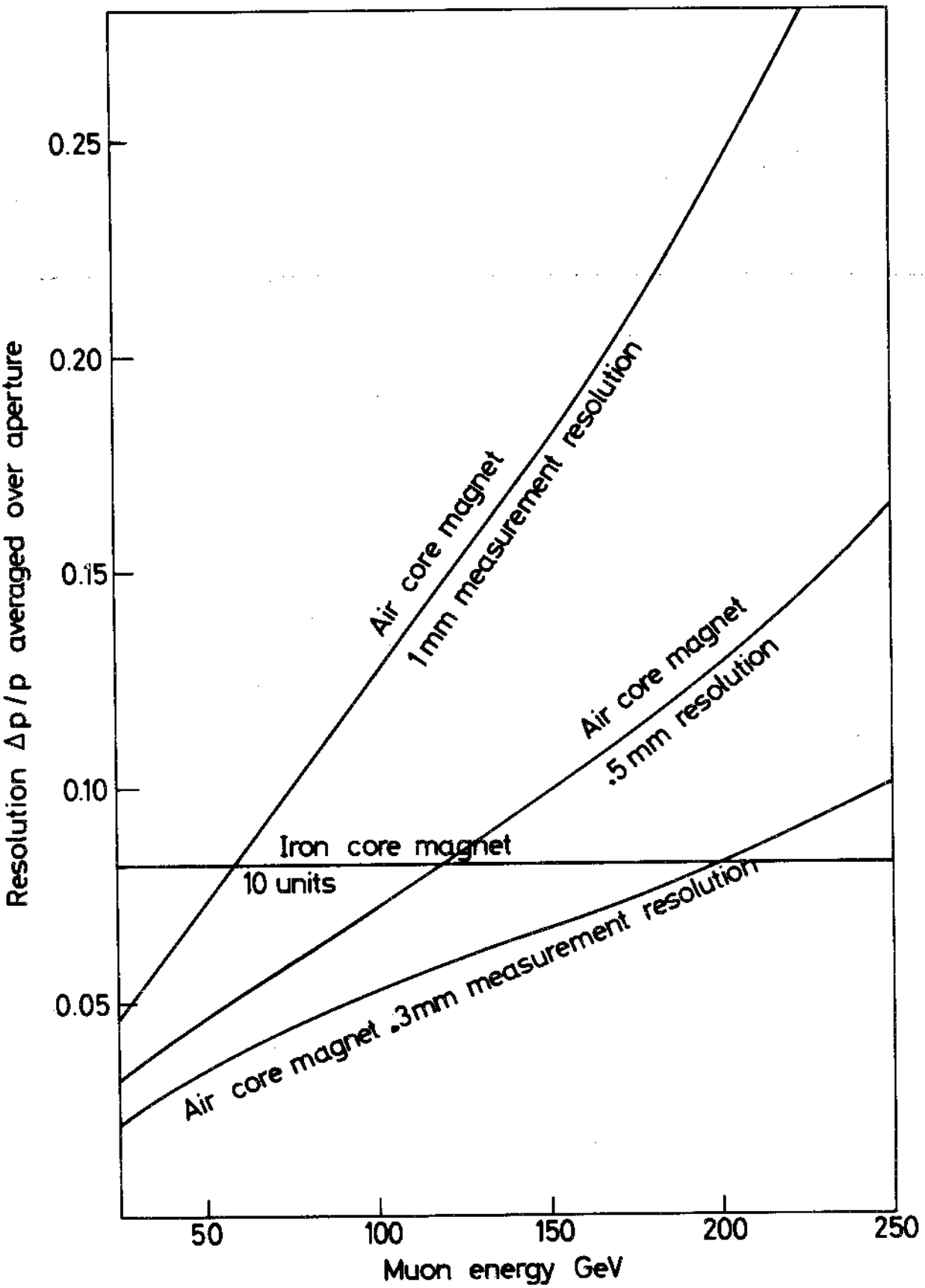

Fig. 15 Muon momentum resolutions for the two proposed magnet schemes

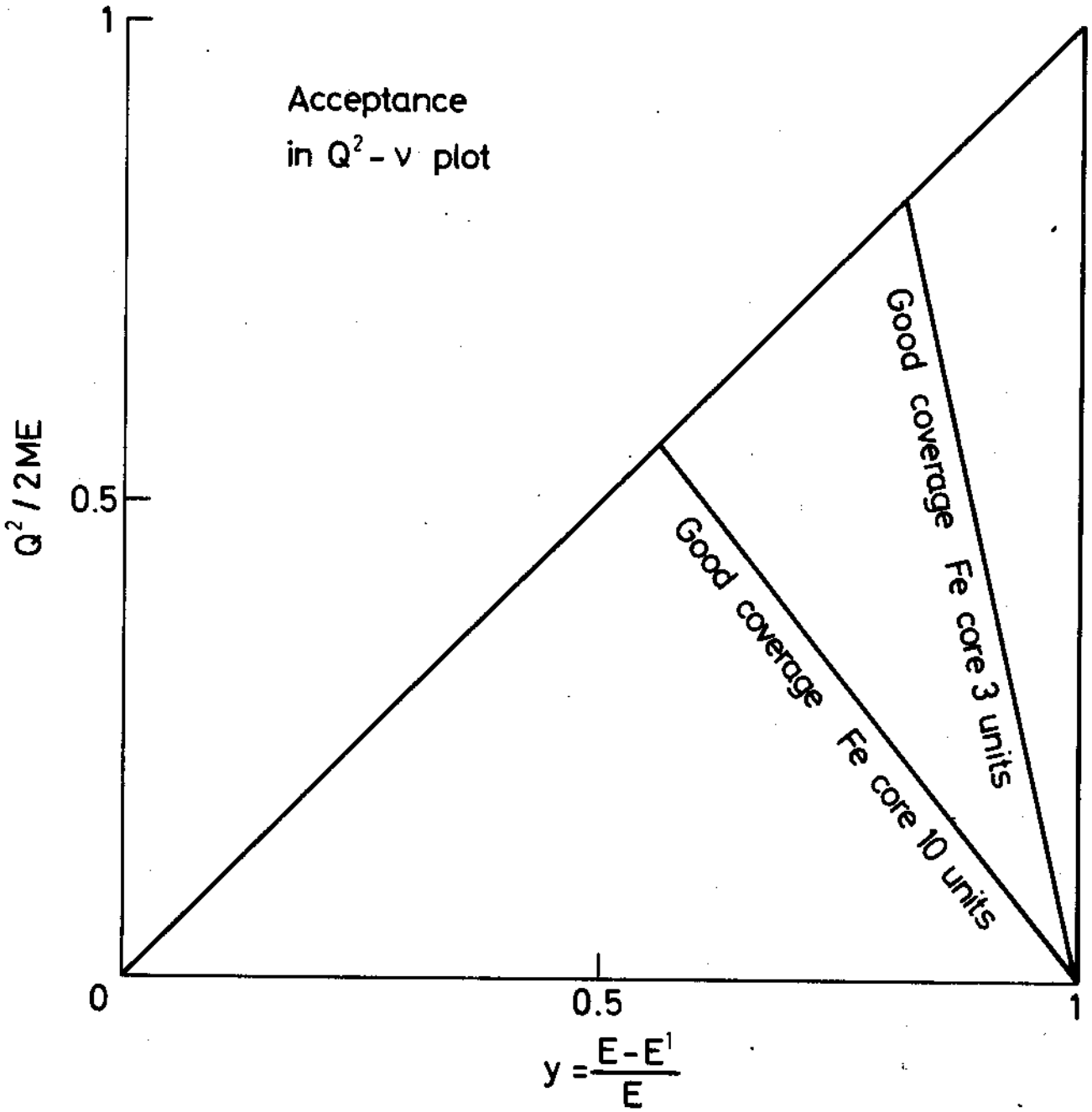

Fig. 16 Acceptance in the Q^2-ν plot for muons originating in the centre of the hadron shower detector at 150 GeV neutrino energy